Chemosphere 346 (2024) 140615

Contents lists available at ScienceDirect

Chemosphere

journal homepage: www.elsevier.com/locate/chemosphere

Effects of meteorological conditions on the mixing height of Nitrogen dioxide in China using new-generation geostationary satellite measurements and machine learning

Naveed Ahmad [a], Changqing Lin [a,*], Alexis K.H. Lau [a,b], Jhoon Kim [c], Chengcai Li [d], Kai Qin [e], Chunsheng Zhao [d], Jintai Lin [d], Jimmy C.H. Fung [a,f], Ying Li [g,**]

[a] Division of Environment and Sustainability, The Hong Kong University of Science and Technology, Clear Water Bay, Hong Kong, China
[b] Department of Civil and Environmental Engineering, The Hong Kong University of Science and Technology, Clear Water Bay, Hong Kong, China
[c] Department of Atmospheric Sciences, Yonsei University, Seoul, 03722, Korea
[d] Department of Atmospheric and Oceanic Sciences, School of Physics, Peking University, Beijing 100871, China
[e] School of Environment and Spatial Informatics, China University of Mining and Technology, Xuzhou, Jiangsu, 221116, China
[f] Department of Mathematics, The Hong Kong University of Science and Technology, Clear Water Bay, Hong Kong, China
[g] Department of Ocean Science and Engineering, Southern University of Science and Technology, Shenzhen 518055, China

HIGHLIGHTS

- Our study comprehensively examined the variations in mixing height of NO_2 in China.
- GEMS shows a good potential to monitor the NO_2 pollution hourly.
- Meteorological conditions have a significant impact on the mixing height of NO_2.
- Machine learning model showed promising results to predict mixing height of NO_2.
- Our results enhance our comprehension of the three-dimensional variations in NO_2.

GRAPHICAL ABSTRACT

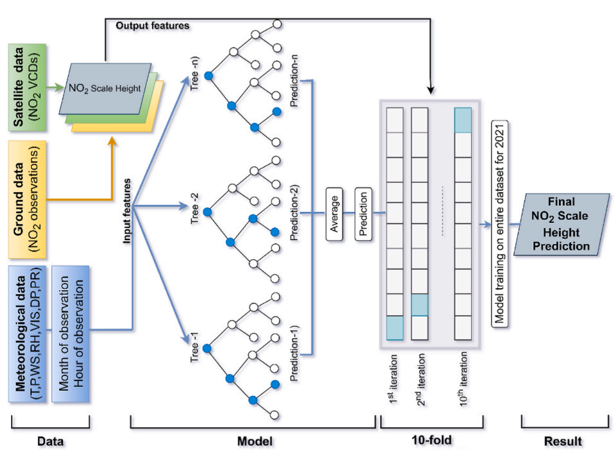

ARTICLE INFO

Handling Editor: Volker Matthias

Keywords:
GEMS
Nitrogen dioxide

ABSTRACT

Nitrogen dioxide (NO_2) plays a critical role in terms of air quality, human health, ecosystems, and its impact on climate change. While the crucial roles of the vertical structure of NO_2 have been acknowledged for some time, there is currently limited knowledge about this aspect in China. The Geostationary Environment Monitoring Spectrometer (GEMS) is the world's first geostationary satellite instrument capable of measuring the hourly

* Corresponding author.
** Corresponding author.
E-mail addresses: cqlin@ust.hk (C. Lin), liy66@sustech.edu.cn (Y. Li).

https://doi.org/10.1016/j.chemosphere.2023.140615
Received 15 July 2023; Received in revised form 4 October 2023; Accepted 2 November 2023
Available online 4 November 2023

Vertical distribution
Meteorology
Machine learning

columnar amount of NO_2. The study presented here introduces the use of mixing height for NO_2 in the atmosphere. A thorough examination of spatiotemporal variations in the mixing height of NO_2 was conducted using data from both the GEMS and ground-based air quality monitoring networks. A random forest model based on machine learning techniques was utilized to examine how meteorological parameters affect the mixing height of NO_2. The results of our study reveal a notable seasonal fluctuation in the mixing height of NO_2, with the highest values observed during the summer and the lowest values during the winter. Additionally, there was an increasing diurnal trend from early morning to mid-afternoon. Moreover, the study discovered elevated NO_2 mixing heights in the dry regions of northern China. The results also indicated a positive correlation between the mixing height of NO_2 and temperature and wind speed, while negative associations were found with relative humidity and air pressure. The machine learning model's predicted NO_2 mixing heights were in good agreement with the measurement-based outcomes, as evidenced by a coefficient of determination (R^2) value of 0.96 (0.84 for the 10-fold cross-validation). These findings emphasize the noteworthy influence of meteorological variables on the vertical distribution of NO_2 in the atmosphere and enhance our comprehension of the three-dimensional variations in NO_2.

1. Introduction

Nitrogen dioxide (NO_2) is of great importance in atmospheric photochemistry and has a significant impact on air quality, human health, ecosystems, and the forcing of climate change (Myhre et al., 2013). Natural sources of NO_2 include soil microbial processes, forest fires, and lightning (Li et al., 2022; van der A. et al., 2008), while vehicles, biomass burning, industries, and power plants are the primary anthropogenic emission sources (Jion et al., 2023). The primary NO_2 sinks include the nighttime hydrolysis of dinitrogen pentoxide (N_2O_5), the daytime conversion of NO_2 to nitric acid (HNO_3), and dry deposition (Jacob, 2000). NO_2 is a major precursor for the synthesis of tropospheric ozone (O_3), as it can alter the concentration of hydroxyl radical (Wang et al., 2022). NO_2 is also a significant contributor to the formation of nitrate aerosols and acid rain (Shah et al., 2020). Furthermore, NO_2 itself is a hazardous air pollutant and can have adverse effects on human health (Zhao et al., 2020). Considering the substantial impact of NO_2 on various atmospheric and health-related processes, accurate detection and a thorough investigation of the spatiotemporal fluctuations in NO_2 are imperative.

The properties of the planetary boundary layer (PBL) play a crucial role in determining the vertical dispersion and horizontal transport of air pollutants, which in turn influence the vertical distribution of NO_2 and its concentration at ground level (Akther et al., 2023; Xiang et al., 2019). For example, in a stable PBL, pollutants such as NO_2 released from the ground are unable to disperse upwards easily, resulting in their accumulation near the ground (Levi et al., 2020). Intense solar heating can cause high temperatures, leading to an unstable PBL that promotes the upward dispersion of air pollutants (Kalmus et al., 2022; Su et al., 2020). The wind field is closely linked to atmospheric stability and can influence pollutant concentrations by altering the dispersion and horizontal transport of pollutants (Yin et al., 2019). Large-scale sinking air motion is often associated with high surface air pressure, which can inhibit the vertical diffusion of pollutants (Chow et al., 2018). The low relative humidity conditions promote the growth and expansion of the PBL, allowing for increased vertical mixing of pollutants. However, high relative humidity levels act as a suppressant, limiting the development of PBL and enhancing the accumulation of pollutants near the ground (Xiang et al., 2019). The dew point impacts surface air pollution levels because of its ability to reflect both temperature and humidity. Therefore, various meteorological factors are considered to have a substantial impact on the vertical distribution of NO_2 and its concentration at ground level (Huang et al., 2021).

Although the critical roles of NO_2's vertical distribution in the atmosphere have been acknowledged for quite some time, there is still a lack of understanding regarding this aspect in China, which had the highest pollution levels globally (Amann et al., 2020). This is primarily attributed to the limited availability of measurements concerning the vertical distribution of NO_2 in the atmosphere. While some studies have employed Multi-Axis Differential Optical Absorption Spectroscopy (MAX-DOAS) measurements to address this issue, more research is required to gain a comprehensive understanding of NO_2's vertical distribution in China. By analyzing the data from a MAX-DOAS system in Beijing, Kang et al. (2021) found that vertical profiles of NO_2 coincided with the variation in the PBL height. Hong et al. (2019) investigated the evolution of vertical profiles of air pollutants in a city in eastern China using a MAX-DOAS system and found that NO_2 concentration exponentially decreased with height. Similar vertical distributions of NO_2 were found at a rural site in the north China plain (Cheng et al., 2022). The MAX-DOAS measurements, however, are extremely sparse. Some other studies have used tower-based and aircraft measurements (Bourgeois et al., 2022; Kang et al., 2021). Tower-based observations are restricted to the immediate vicinity of the tower and are typically available only within a few hundred meters of the ground, depending on the tower's height (Li et al., 2020). While aircraft-based measurements can capture data at various heights, they may not be suitable for continuous monitoring due to their limited availability.

Satellite instruments offer air quality monitoring with broad spatial coverage (Li and Managi, 2022). Satellite-retrieved vertical column densities (VCDs) of NO_2 have been extensively utilized to identify variations in NO_2 pollution and NO_x emissions across various regions (Chong et al., 2016; Park et al., 2021; Wang et al., 2023). Over the past decades, the VCDs of NO_2 have been continuously monitored by the polar sun-synchronous low earth orbiting (LEO) satellite instruments, such as the Global Ozone Monitoring Experiment (GOME), the Scanning Imaging Spectrometer for Atmospheric Chartography (SCIAMACHY), the GOME-2, the Ozone Monitoring Instrument (OMI), the Ozone Mapping Profiler Suite (OMPS), the Tropospheric Monitoring Instrument (TROPOMI), and the Environmental Trace Gasses Monitoring Instrument (EMI) (Flynn et al., 2014; Iqbal et al., 2022; Veefkind et al., 2012; Zhang et al., 2018).

The Geostationary Environment Monitoring Spectrometer (GEMS) is the first satellite instrument specifically designed to monitor both gaseous and aerosol pollutants from a geostationary earth orbit (GEO) over Asia (Kim et al., 2020). GEMS was launched successfully by the Republic of Korea on February 19, 2020, and entered its intended orbit on March 6, 2020. The primary aim of the GEMS mission is to provide hourly columnar measurements of key air quality parameters, including NO_2, O_3, and aerosols over Asia. Compared to traditional LEO satellite instruments, the GEO-based GEMS monitors the columnar amount of air pollutants more frequently, improving our understanding of the diurnal variation of NO_2 over Asia (Yang et al., 2023). The measurements provided by GEMS offer significant improvements over ground-based fixed-site measurements in terms of spatial coverage.

Mixing height is a crucial parameter that characterizes the vertical structure of the atmosphere. Initially introduced for aerosols, it represents the equivalent depth of the aerosol layer near the ground (Koelemeijer et al., 2006; Liu et al., 2005). The mixing height of an air pollutant represents the height at which the pollutant can be vertically dispersed in the atmosphere. Examining the mixing height of NO_2 can provide valuable insights into the vertical structure of NO_2 in the atmosphere. In this study, we comprehensively investigated the spatio-temporal variation in the mixing height of NO_2 over China using data from the new-generation Geostationary satellite (i.e., GEMS) and ground monitoring networks. We also analyzed the relationships between the mixing height of NO_2 and various meteorological parameters. Further, we employed a machine learning model to predict NO_2 mixing heights based on meteorological parameters. By combining observational and modelling approaches, this study aimed to enhance our understanding of the vertical structure of NO_2 in the atmosphere over China.

2. Data and methodology

2.1. Study area

This study aims to investigate the spatial and temporal variations in NO_2 using satellite and various ground measurements across China. The study area is illustrated in Fig. S1, covering most of China between 17°N and 45°N, and 78°E and 130°E. In recent years, China's rapid industrialization and economic growth have led to a significant increase in energy consumption. The country's rapidly expanding economy is heavily dependent on the use of fossil fuels, resulting in substantial emissions of air pollutants (Wang et al., 2019). As a result, due to high levels of air pollution caused by significant emissions of pollutants such as NO_2, China has become one of the most highly air-polluted nations in the world.

2.2. Satellite-based NO_2 measurements

To obtain the VCDs of NO_2 over the study region for the year 2021, we utilized measurements from the GEMS and its level 2 product. The algorithm employed to retrieve the VCDs of NO_2 is based on the differential optical absorption spectroscopy (DOAS) technique (Platt et al., 2008). Initially, the algorithm calculates the slant column densities (SCDs) of NO_2 using the optical fitting interval in the wavelength range of 432–450 nm. The SCDs are then converted to VCDs using hourly air mass factors (AMFs). The nominal detection limit for the VCDs of NO_2 product is 1×10^{14} molec/cm^2. The accuracy of the satellite retrieval is estimated to be 1×10^{15} molec/cm^2. Any VCDs of NO_2 beyond the GEMS detection limit of greater than 1×10^{17} molec/cm^2 were considered noise and were thus removed for further analysis.

GEMS is designed with various scanning modes, including "Half East", "Nominal Daily", "Full Central", "Full West", and "Half West", to monitor air quality with different spatial extents at various times of the day. The nominal spatial resolution of the GEMS dataset is approximately 7 km × 7.7 km, by binning two pixels of 3.5 km × 7.7 km each. The satellite measurement pixels are irregular in shape due to the nature of East-to-West scans over the globe. However, in this study, we re-gridded the VCDs of NO_2 from GEMS onto a regular grid of 0.2° × 0.4° with the same spatial extent, regardless of the GEMS scanning modes, from 08:00 a.m. to 15:00 p.m. (China's local time in UTC+8 was used in this study). Due to the high uncertainty associated with satellite observations under cloudy conditions, data with a cloud fraction of less than 30 % were considered for further analysis to maintain the balance between adequate measurements while reducing the influences of cloud-contaminated data. Furthermore, data with a solar zenith angle larger than 70° were also excluded. The sample size of satellite data for each hour from 08:00 a.m. to 15:00 p.m. in the study region for the year 2021 is shown in Fig. S2. Overall, the sample size of satellite data increased in the morning and decreased in the afternoon. Detailed information on the GEMS mission and retrieval algorithms of its products can be found in the study by Kim et al. (2020).

2.3. MAX-DOAS measurements

To assess the accuracy of the satellite-retrieved VCDs of NO_2, we obtained column NO_2 data from a MAX-DOAS system situated in Xuzhou in eastern China (34.210° N and 117.140° E). MAX-DOAS measurements were taken during January 1–7, April 1–7, July 25–31, and October 15–21 of 2021 to evaluate the uncertainties of the satellite measurements in the four seasons. The MAX-DOAS technique employs various elevation angles, ranging from 0 to 90°, to measure the scattered sunlight in the visible and ultra-violet spectral ranges. It can simultaneously measure the column amounts of several trace gases, including NO_2 (Kreher et al., 2020).

2.4. Ground-based NO_2 measurements

This study obtained the hourly NO_2 concentration data throughout the year 2021 from ground air quality monitoring networks in the study region. As shown in Fig. S1, the NO_2 concentration data at 1645 stations were collected from China National Environmental Monitoring Center (http://www.cnemc.cn), the Hong Kong Environmental Protection Department (https://cd.epic.epd.gov.hk/EPICDI/air/), and the Taiwan Environmental Protection Administration (http://210.69.101.63/taqm/en/default.aspx). According to the technical standards, the instruments for monitoring pollutant concentrations are correctly operated and maintained for data assurance and quality control (Zhang and Cao, 2015).

2.5. Ground-based meteorological measurements

The meteorological variables, including temperature (T), air pressure (P), wind speed (WS), relative humidity (RH), dew point (DP), visibility (VIS), and precipitation (PR) in the study region for the year 2021 were acquired from the global telecommunications system of the World Meteorological Organization. As shown in Fig. S1, the meteorological data at 208 stations were used in this study. Most meteorological stations are situated in open areas to monitor regional weather conditions.

2.6. Upper-air radiosonde measurements

To assess the mixing height of NO_2, this study estimated the daily noontime mixing layer height (MLH) using upper-air radiosonde measurements of meteorological values at Beijing meteorological station (116.58 °E, 40.07 °N). The radiosonde measurements were available at 8:00 a.m. and 8:00 p.m. The parcel method was employed to estimate the noontime MLH (Holzworth, 1964). This method assumes that the potential temperature within the mixing layer remains constant. Therefore, the MLH can be identified as the height at which the ambient potential temperature is equal to the surface potential temperature. Then, the noontime average of the MLH between 12:00 p.m. and 14:00 p.m. were obtained. This method has been applied in many previous studies in China (Su et al., 2017; Lin et al., 2021).

2.7. Location matching between satellite and ground measurements

Satellite measurements have a large spatial coverage, whereas ground measurements are available at specific locations. To pair up the data from satellite measurements and ground air quality monitoring networks, satellite NO_2 data for the exact locations corresponding to ground stations were extracted. The locations of the meteorological stations also differ from air quality monitoring stations. To facilitate the analysis of the impacts of meteorological conditions on air pollution, we assigned the meteorological data to the air quality monitoring stations located within a 50 km radius of the meteorological station. The stations were filtered based on valid observations of all meteorological and air quality variables. Eventually, the complete sets of data at 1273 stations were used in this study.

2.8. Mixing height of NO_2

The unit for the satellite-derived VCDs of NO_2 is molec/cm^2, while the ground-level NO_2 concentration (C_g) is in μg/m^3. Equation (1) converts the satellite VCDs of NO_2 from molec/cm^2 to μg/m^2:

$$VCD_{NO2}\left(\frac{\mu g}{m^2}\right)=\frac{VCD_{NO2}\left(\frac{molec}{cm^2}\right)\times M_{NO2}\left(\frac{g}{mol}\right)}{N_A\left(\frac{molec}{mol}\right)}\times 10^{10} \quad (1)$$

where M_{NO2} is the molar mass of NO_2, and N_A is the Avogadro's number. Then, the mixing height (H) of NO_2 can be estimated from the ratio of satellite-based VCDs of NO_2 and ground-level NO_2 concentration in the same physical units:

$$H(m)=\frac{VCD_{NO2}\left(\frac{\mu g}{m^2}\right)}{C_g\left(\frac{\mu g}{m^3}\right)} \quad (2)$$

2.9. Machine learning model

In this study, we investigated the relationship between meteorological values and the mixing height of NO_2. We utilized a machine learning-based random forest (RF) regression model to predict the mixing height of NO_2 from meteorological values. The RF regression model approximates a function that represents the connection between the input and output datasets using linear and non-linear regressions. It was used to learn the relationships between the surface meteorological values and the mixing height of NO_2. The RF regression algorithm is a tree-based ensemble learning method that can perform regression and classification using multiple decision trees and the bootstrap and aggregation technique. It involves a set of regression trees trained through bootstrap sampling, and the final output is the average of the outputs from individual trees. Additional details on the RF regression model can be found in Hastie et al. (2008). The model training used nine predictors, including seven meteorological variables (i.e., T, P, WS, RH, DP, VIS, and PR) together with two time variables, including hour of the day (8 a.m.–15 p.m.) and month of the year (1–12) corresponding to the available observations for the meteorological variables. The RF regression model formulates the mixing height of NO_2 as a function of all input parameters.

To evaluate the model performance, we employed the 10-fold cross-validation technique. We divided the training dataset into 10 groups of similar size. Of the 10 folds, nine were used for model fitting, while the remaining one was used for validation to test the model performance. These steps were repeated ten times to test the model performance for each fold. A set of commonly used statistical indicators, including coefficient of determination (R^2), root mean squared error (RMSE), mean deviation (MD), and mean absolute percentage error (MAPE), were adopted to test the model performance during the cross-validation. Besides the cross-validation, the RF regression model was trained to predict the mixing height of NO_2 based on the entire dataset for 2021. The fully trained model was then evaluated using the same statistical indicators as the cross-validation.

3. Results

3.1. GEMS NO_2 VCDs

We first analyzed the VCDs of NO_2 from GEMS measurements. Fig. 1 shows spatial distributions of the annual mean of NO_2 VCDs for 2021 in China and its four major city clusters: Beijing-Tianjin-Hebei (BTH), Yangtze River Delta (YRD), Pearl River Delta (PRD), and Sichuan Basin (SCB). Human activities have a significant impact on NO_2 pollution. Elevated levels of NO_2 pollution were found in the four city clusters, which are densely populated areas with intensive industrial activities and heavy traffics. Furthermore, the NO_2 densities in eastern China were found to be an order of magnitude higher than those in western China. These findings suggest that eastern China had significantly higher NO_x emissions from human activities compared to western China. Fig. S3 shows seasonal variations in the satellite-derived VCDs of NO_2 for 2021 in the study region. Typically, NO_2 densities reach their maximum in winter and minimum in summer. Elevated NO_2 densities during winter are attributed to a low PBL and a stable atmosphere, which are unfavorable for the dispersion of air pollutants.

3.2. Evaluation of GEMS NO_2 VCDs

The ground-based MAX-DOAS measurements, which are a well-

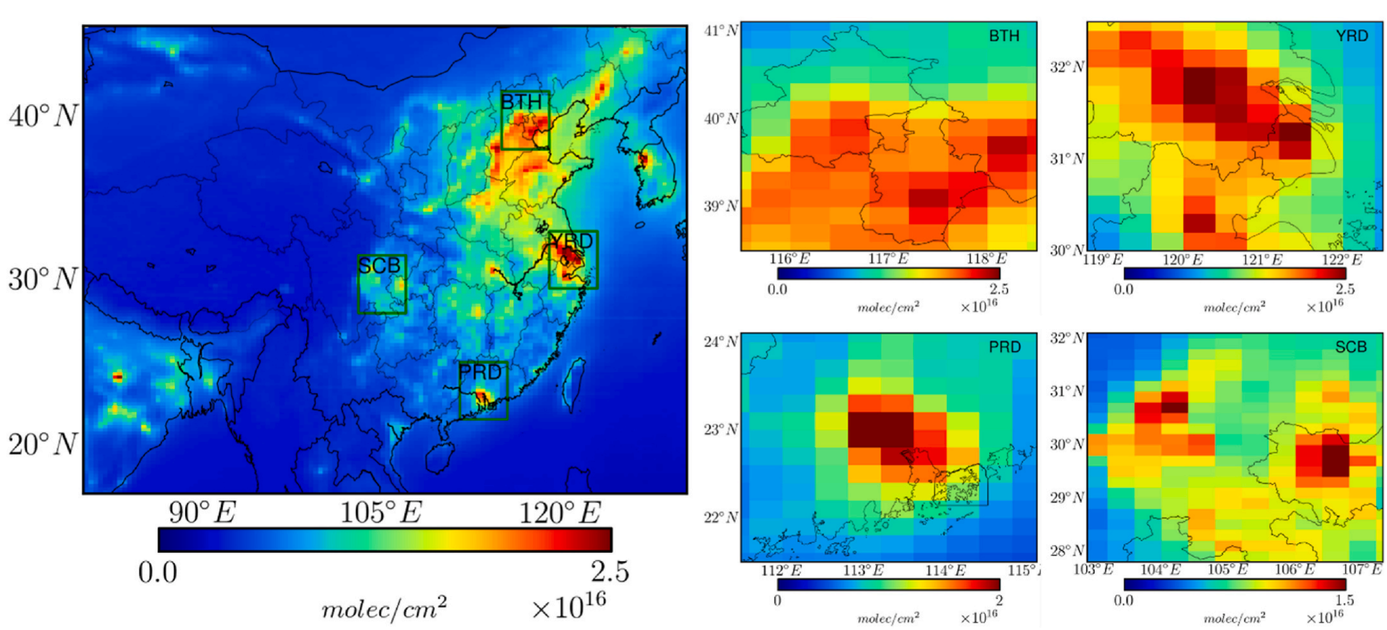

Fig. 1. Spatial distributions of annual mean of the VCDs of NO_2 from GEMS for 2021 in the study region (left panel) and in the four major city clusters in China (right panel): Beijing-Tianjin-Hebei (BTH), Yangtze River Delta (YRD), Pearl River Delta (PRD), and Sichuan Basin (SCB).

established technique, were utilized to validate the satellite observations. Fig. S4 shows a comparison of the hourly VCDs of NO_2 from GEMS with the data retrieved by the MAX-DOAS in Xuzhou of China. A comparison was conducted for all four seasons, including periods with both high and low NO_2 concentrations, using both instruments. The variations in NO_2 were accurately detected by both the satellite and MAX-DOAS measurements in all seasons. Both instruments recorded the highest VCDs of NO_2 in winter due to the stable atmospheric conditions. Conversely, both measurements observed the lowest VCDs of NO_2 in summer due to the strongest vertical dispersion and photochemical NO_2 destruction. A good correlation (R = 0.82) was found between the GEMS and MAX-DOAS measurements. Some deviations were observed between the two datasets. Specifically, the VCDs of NO_2 from GEMS were higher than ground measurements under clean conditions and lower than ground measurements under polluted conditions. These deviations may be attributed to differences in the spatial representativeness of the two datasets. Satellite measurements have a larger footprint, considering the average NO_2 concentration within the pixel, while MAX-DOAS measurements are point observations. These deviations are in agreement with the validations of other satellite instruments, such as TROPOMI (Karagkiozidis et al., 2023).

The GEMS columnar measurements were then compared with ground-level NO_2 concentration measured by air quality monitoring networks across China. Fig. S5 compares the monthly mean of GEMS-derived VCDs of NO_2 and ground-based NO_2 concentrations in four major cities in the study region, i.e., Beijing, Shanghai, Hong Kong, and Lhasa. The monthly averages displayed a strong agreement between satellite-derived and ground-based NO_2 for the three major cities in eastern China, with correlation coefficients of 0.76, 0.73, and 0.90 for Beijing, Shanghai, and Hong Kong, respectively. The same seasonal variation patterns were observed, with the highest values in winter and the lowest in summer. However, in Lhasa, a key city on the Tibetan Plateau, the GEMS-derived VCDs of NO_2 and ground-based NO_2 concentrations showed opposite seasonal variations. The maximum VCDs of NO_2 were observed during the summer, while the reverse pattern was observed for the ground-level NO_2 concentration. This difference is due to the impacts of natural emissions, such as lightning in summer, which release NO_2 in the upper layer (Guo et al., 2017). The lightning activity is one of the main sources of NO_2 and is strongly associated with the upper tropospheric NO_2 over the Tibetan Plateau.

Fig. 2(a) plots the spatial distribution of the correlation coefficient between satellite-based hourly NO_2 VCDs and ground-based hourly NO_2 concentrations in China for 2021. The corresponding sample sizes are shown in panel (b). The satellite-derived VCDs of NO_2 display positive correlations (R > 0.4) with ground-level concentrations in most regions of China. These evaluations demonstrate the good capability of GEMS for continuous monitoring of NO_2 on an hourly basis. However, it should be noted that negative correlations were detected over the Tibetan Plateau region, which could be related to the high emissions from lightning in the upper air during summer.

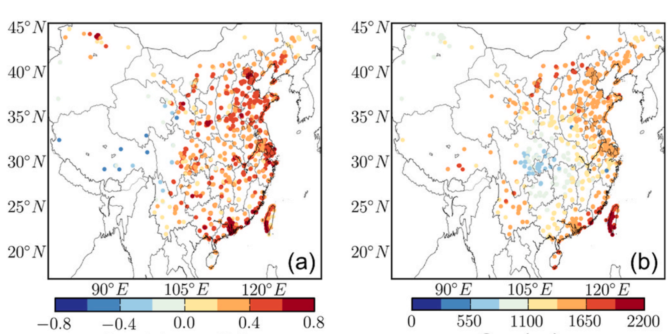

Fig. 2. Panel (a) shows spatial distribution of correlation coefficient between satellite-based hourly NO_2 VCDs and ground-based hourly NO_2 concentrations for 2021. Corresponding sample sizes are shown in panel (b).

3.3. NO_2 mixing height

Based on Equation (2), the mixing height of NO_2 was estimated from satellite and ground measurements. The time series of the daily mean mixing height of NO_2 in Beijing is shown in Fig. 3(a). It demonstrates a distinct seasonal pattern with the lowest levels during winter, succeeded by an increasing trend during the first half of the year and a decreasing pattern during the second half of the year. The annual mean NO_2 mixing height was 1072 m. These findings suggest that the meteorological conditions favour the vertical diffusion of NO_2 in the boundary layer in the summer. By contrast, the low mixing height of NO_2 during winter resulted from stable atmospheric conditions, which were unfavorable for the vertical diffusion of NO_2. As a result, a majority of pollutants accumulated near the ground, resulting in high surface-level NO_2 concentrations. To evaluate the variation of the mixing height, Fig. 3(b) shows the time series of daily noontime MLH estimated from the upper-air radiosonde measurements in Beijing. A good agreement with a correlation coefficient of 0.65 was found between the two data sets, indicating accurate estimation of the NO_2 mixing height.

Spatial distributions of the seasonal average of the mixing height of NO_2 across the study region are depicted in Fig. 4. On a national average, the seasonal mean of NO_2 mixing height was highest in summer (876 m), followed by spring (739 m) and autumn (688 m), while the minimum was observed during winter (581 m). In addition, elevated values were found over the dry northern regions. These results are similar to the previous investigations of spatiotemporal variation in the PBL height using reanalysis data and sounding observations in China (Guo et al., 2016). Their study showed that the PBL heights in spring and summer are generally higher than those in autumn and winter. Further, the elevated PBL heights were also found over the dry northern regions, which could result from the influences of hydrologic factors (e.g., low humidity and solar radiations) that modulate the PBL height (Seidel et al., 2012; Guo et al., 2016).

Based on the hourly measurements, Fig. 5 depicts the spatial distributions of the average NO_2 mixing height for each hour from 08:00 a.m. to 15:00 p.m. in the study region in 2021. The mixing height of NO_2 was observed to increase from early morning to mid-afternoon. On a national average, the NO_2 mixing height was at its minimum at 08:00 a.m. (497 m) and reached its maximum at 15:00 p.m. (1093 m). The increased mixing height of NO_2 during noontime and early afternoon can be related to the enhanced vertical diffusion of NO_2 resulting from meteorological factors that are responsible for the daytime development of the PBL. For instance, the availability of strong solar radiation could increase ground temperature and enhance wind speed during noontime and early afternoon. These changes result in an unstable atmosphere, which promotes the vertical dispersion of air pollutants.

3.4. Effects of meteorological conditions on the mixing height of NO_2

We used Hong Kong as an example to demonstrate the effects of meteorological conditions on the variation in the mixing height of NO_2. Fig. S6 shows the time series of the daily mean of the NO_2 mixing height and various meteorological parameters (e.g., T, P, WS, RH, DP, VIS, and PR) for Hong Kong in 2021. During the summer of 2021, from 17 July to 10 August (as highlighted in the black rectangle), the NO_2 mixing height demonstrated a decline. During this period, the daily mixing height of NO_2 decreased to a level below 300 m in Hong Kong. Upon zooming in on this specific time period, a similar variation was observed between the NO_2 mixing height and surface air pressure, as shown in Fig. S7. The declines in the mixing height of NO_2 and air pressure during this period indicate the effects of sinking air motion on outer edges of a tropical cyclone (a low-pressure system, see Fig. S8) located near Hong Kong. The subsidence effect of tropical cyclone suppresses the development of the PBL in its periphery, thereby reducing the vertical dispersion of air

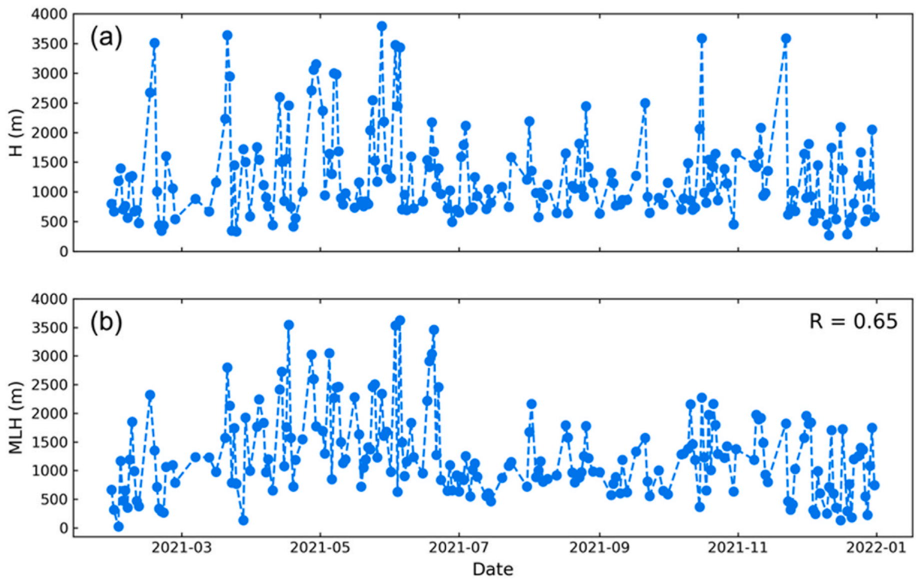

Fig. 3. Time series of daily mean (12 p.m.–02 p.m.) (a) NO_2 mixing height (H) and (b) mixing layer height (MLH) in Beijing for 2021.

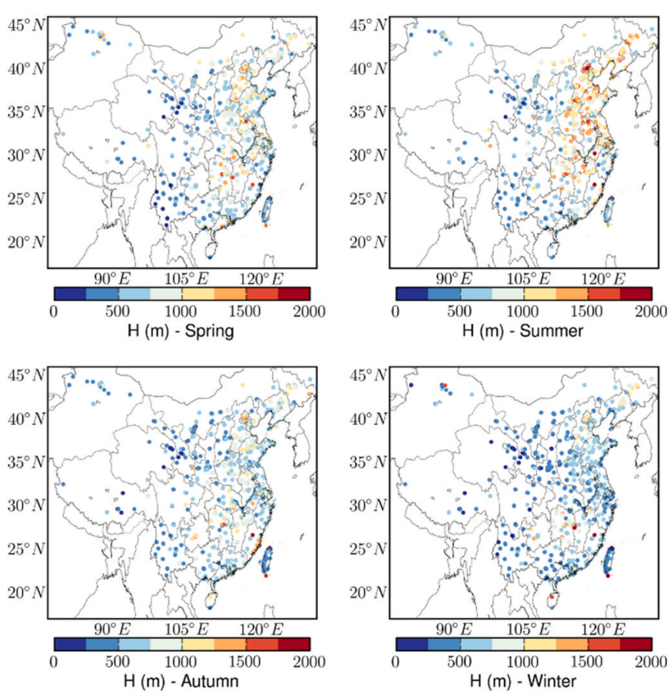

Fig. 4. Spatial distributions of seasonal mean of NO_2 mixing height (H) in the study region in 2021.

pollutant and the mixing height of NO_2. Such a meteorological condition is often conducive to the occurrence of severe air pollution episode on the ground in this region (Chow et al., 2018). These results indicate that weather conditions greatly influence the development of NO_2 mixing height.

Considering the spatial heterogeneity in the meteorological effects on the development of the vertical structure of NO_2, we extended our analysis to the entire study region. Fig. 6 plots the geographic distribution of the correlation coefficient between the NO_2 mixing height and meteorological parameters (e.g., T, P, WS, RH, DP, VIS, and PR) in 2021. Overall, the analysis demonstrated that temperature, wind speed, dew point, and visibility had positive correlations with the NO_2 mixing height, while relative humidity and air pressure mainly demonstrated an inverse relationship. Precipitation showed a limited impact on the development of the NO_2 mixing height. The atmosphere's dynamic and thermodynamic aspects played crucial roles in the development of the vertical structure of NO_2 across the study region. The positive relationships between the temperature and the NO_2 mixing height show that by increasing temperature, the NO_2 mixing height would increase. We have seen similar behaviour from the daytime development of the mixing height of NO_2 (Section 3.3), which increased from early morning to the afternoon as the day progressed. In addition, the NO_2 mixing height would increase with increased wind speed, improved visibility, and increased dew point, while it would decrease with increased relative humidity and air pressure. The increased wind speeds are often associated with an unstable atmosphere, which facilitates the momentum transport from the free atmosphere to the ground. Elevated surface air pressures are often associated with sinking air motion and the air divergence near the ground, leading to a stable atmosphere that influences the vertical distribution of NO_2.

3.5. *Prediction of the NO_2 mixing height*

The RF regression model was applied to estimate the mixing height of NO_2 from the meteorological values. Fig. 7(a) shows the 10-fold cross-validation of the mixing height of NO_2 from machine learning against measurement-based results. It can be seen that our model has achieved a good R^2 score of 0.84 for the 10-fold cross-validation. The RMSE and MAPE were 224.99 m and 18.14 %, respectively. The results showed a low bias, with a mean deviation of 1.77 m. Then, the model was trained on the whole dataset. The results are presented in Fig. 7(b). Applying the RF regression model to the whole data set has shown an improved R^2 value of 0.96 between the prediction- and measurement-based NO_2 mixing heights. Here, the RMSE and MAPE were further improved to 115.19 m and 9.16 %, respectively. The full model has shown a mean deviation of 0.77 m, which depicts a low bias and uncertainty. These results show that the input variables used in this study have a good capability of predicting the mixing height of NO_2.

To explore the contributions of individual explanatory variables in the RF regression model, their feature importance in descending order is presented in Fig. S9. The month of the year was the most important variable in this model, with a feature importance of 23.70%. It represents intra-annual variability in the mixing height of NO_2, with low values in the cold season and high values in the warm season. The following important variables were DP, P, T, VIS, RH, and WS, all of

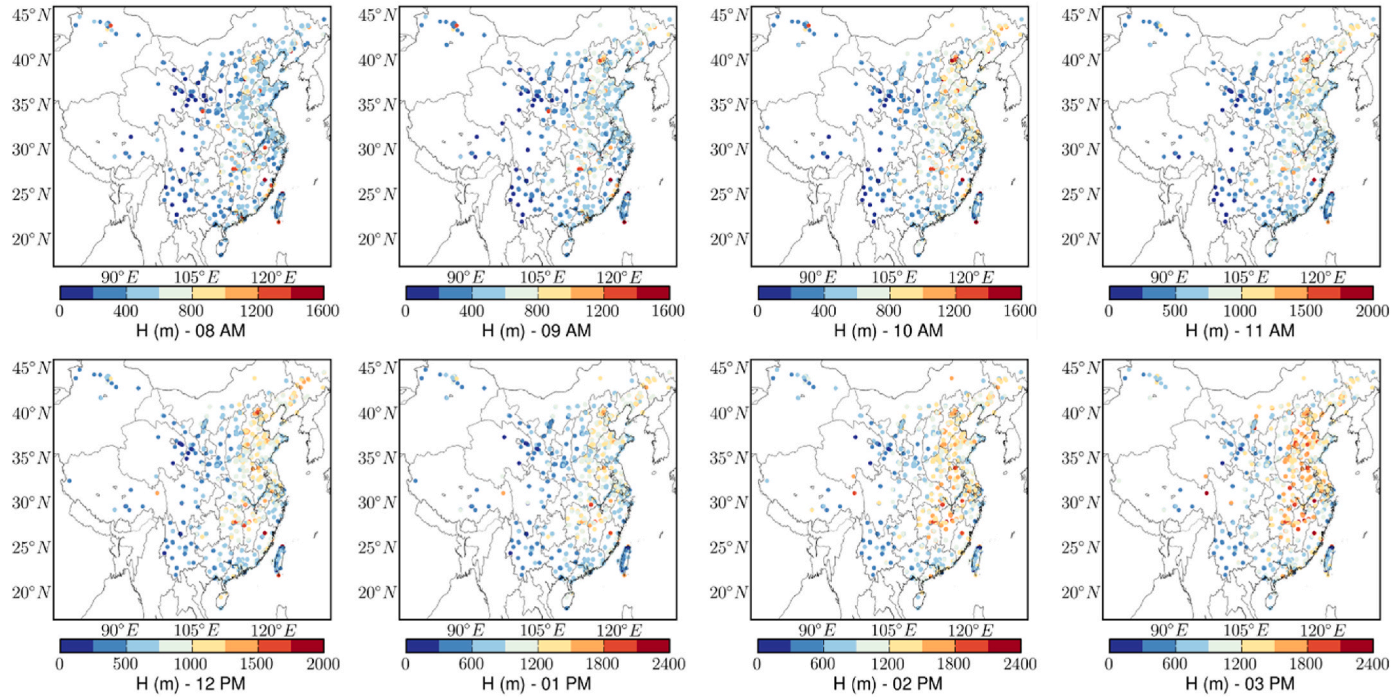

Fig. 5. Spatial distributions of the average NO_2 mixing height (H) for each hour from 08:00 a.m. to 15:00 p.m. in the study region in 2021.

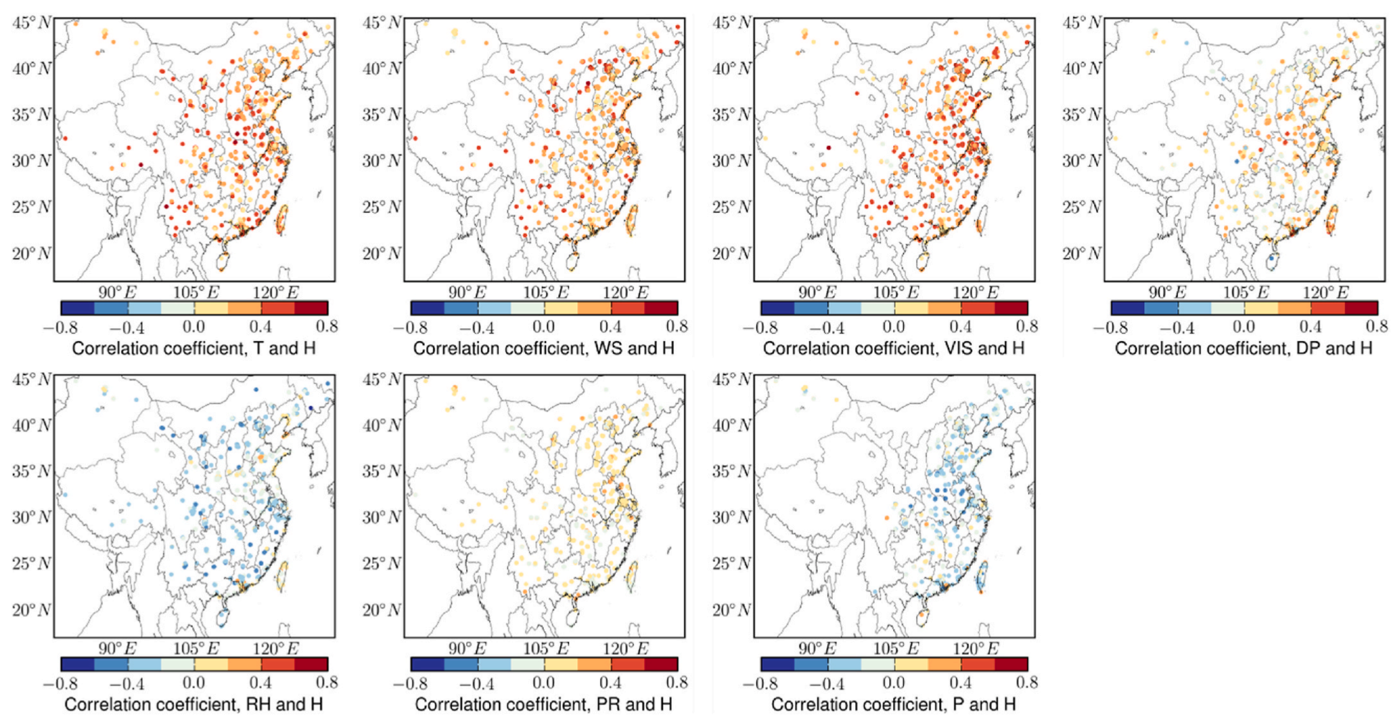

Fig. 6. Spatial distributions of the correlation coefficient between hourly NO_2 mixing height (H) and meteorological parameters, including temperature (T), wind speed (WS), visibility (VIS), dew point (DP), relative humidity (RH), precipitation (PR) and air pressure (P), for 2021.

which are critical meteorological parameters for the development of the NO_2 mixing height. The hour of the day was the second to last feature in terms of importance, which could be attributed to the diurnal development of the vertical structure of NO_2. Precipitation had the least contribution to the model, with an importance of 3.27 %. It is pertinent to mention that the prediction of the mixing height of NO_2 is not dependent on any individual meteorological parameter, but rather on each parameter's contribution.

4. Discussion

The use of GEMS, a new-generation geostationary satellite instrument, offers a new opportunity to monitor air quality over a large region with unprecedented spatial and temporal resolution. The quality of the GEMS measurements was evaluated against ground-based measurements from a MAX-DOAS system and air quality monitoring networks. A good correlation of 0.82 (N = 63) was found between the columnar

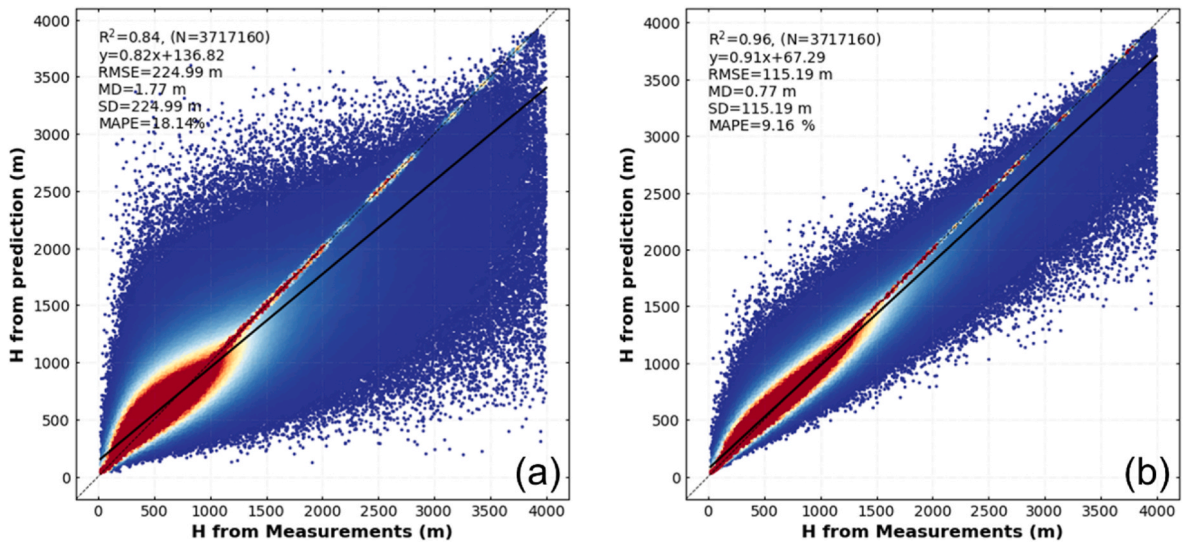

Fig. 7. (a) The 10-fold cross-validation of the NO_2 mixing height from the machine learning against those obtained from measurements. (b) The validation of the NO_2 mixing height from the machine learning model trained on the entire dataset for 2021.

measurements from GEMS and the MAX-DOAS system. Deviations between the two datasets can be caused by differences in spatial representativeness. Additionally, the column densities of NO_2 from GEMS measurements were highly correlated with ground-based NO_2 concentrations from air quality monitoring networks across China. These evaluations demonstrate the capability of GEMS for continuous monitoring of the VCDs of NO_2 on an hourly basis. However, since the MAX-DOAS measurement data were only available for a week in each season, comprehensive evaluations against the MAX-DOAS measurements in different locations across the study region are necessary. These evaluations can be conducted in the future when sufficient MAX-DOAS measurements across China are available.

In this study, we proposed to combine the column densities from GEMS and ground-level concentration to reveal the vertical structure of NO_2 over a large region. When column densities are similar, high ground-level concentrations indicate that the majority of pollutants are accumulated near the ground. Based on this concept, the mixing height of NO_2 was introduced to indicate the vertical structure of NO_2 in this study. The spatiotemporal variation in the mixing height of NO_2 and its influencing factors were then evaluated. Specifically, the impacts of meteorological values on the mixing height of NO_2 were explored. These investigations enhanced our understanding of the three-dimensional variations in NO_2 and its impacts on the occurrence of severe air pollution episode on the ground.

MAX-DOAS measurements can provide similar knowledge on the vertical structure of NO_2, but their measurements are still sparse. Due to the high costs, these measurements do not meet the needs for continuous monitoring over a large region such as China. It is difficult to have an overall picture of the vertical structure of NO_2 across China based only on fixed-site measurements. Given the significant variability in NO_2 across China, it is essential to use alternative methods, such as satellite remote sensing, which have a large spatial coverage. The investigations in this study demonstrate a significant improvement over traditional fixed-site measurements in terms of spatial coverage.

Based on the large-scale measurements from GEMS, the spatial disparity of the density of NO_2 across China was evaluated. The densities of NO_2 in eastern China were an order of magnitude higher than those in western China, implying high anthropogenic emissions from human activities in the eastern region. Western China, such as the Tibetan Plateau, depicted low NO_2 pollution as it had limited industrial production and is sparsely populated. In addition, the VCDs of NO_2 depicted opposite seasonal trends between eastern China and the plateau in western China. In eastern China, the maximum NO_2 amounts were detected during the winter. In contrast, the reverse patterns were observed on the plateau in western China. This is mainly caused by the increased NO_2 production from lightning in the upper layer of the troposphere on the plateau in western China. Due to the limited vertical sensitivity, ground stations cannot detect the increased NO_2 presented in the upper layer of the troposphere.

The mixing height of NO_2 reached the maximum in summer and the minimum in winter. Strong solar heating in summer increases the ground temperature, thereby enhancing the vertical mixing of NO_2 in the boundary layer. Conversely, lower temperatures in winter tend to suppress the vertical mixing of NO_2. Strong wind speeds are often associated with an unstable atmosphere in summer, which in turn increases the mixing height of NO_2. Moreover, the seasonal shift of large-scale high/low-pressure systems can either suppress or facilitate the vertical mixing height of air pollutants through associated descending and ascending motion. In winter, high-pressure systems over the continents are typically associated with sinking air motion and stable atmospheric conditions, resulting in a shallow mixing height of NO_2. Our results indicate a positive correlation between vertical mixing height and dew point, as well as a negative correlation with relative humidity. This suggests that NO_2 vertical mixing increases with higher dew point levels in summer and decreases with higher relative humidity levels in winter.

In addition, the mixing height of NO_2 increased from early morning to the afternoon. The development of NO_2 mixing height is greatly affected by weather parameters, such as temperature, wind speed, and air pressure. These meteorological parameters affect the vertical structure of NO_2 by changing the vertical dispersion and horizontal transport of air pollutants in the PBL. The temperature, wind speed, dew point and visibility showed a positive correlation coefficient with the vertical mixing height of NO_2. The positive relationship between the vertical mixing of NO_2 and temperature is primarily driven by atmospheric thermal processes. As surface heating increases, the air in the adjacent layer becomes heated and expands, leading to a decrease in density. This reduced density makes the air buoyant, causing it to rise and carry the NO_2, resulting in higher vertical mixing of NO_2. Higher wind speeds are associated with greater momentum transfer from the free atmosphere to the ground, leading to an unstable atmosphere and increased vertical mixing of NO_2. As a result, the correlation between wind speed and vertical mixing of NO_2 is positive. The negative correlation between the vertical mixing of NO_2 and pressure is primarily due to higher-pressure atmospheric systems being often associated with descending air and stable atmospheric conditions. These conditions inhibit the vertical transport of pollutants, resulting in a lower vertical mixing of NO_2. Higher relative humidity indicates a greater moisture content in the air, which can contribute to increased aerosol extinction of sunlight. This, in turn, leads to lower vertical mixing of NO_2 and a negative correlation coefficient between the mixing height of NO_2 and relative humidity.

In the short-term period, the mixing height of NO_2 is significantly affected by specific weather systems, such as tropical cyclone. The machine learning-based RF regression model was then used to predict the mixing height of NO_2 from various meteorological values, month of the year and hour of the day. The estimated feature importance of the input predictor variables revealed valuable insights. Among these variables, the month of the year emerged as the most significant, with a feature importance of 23.70%. This variable captures the intra-annual variability in the mixing height of NO_2, displaying lower values during the cold season and higher values during the warm season. Other crucial meteorological parameters for the development of the NO_2 mixing height include dew point, air pressure, temperature, visibility, relative humidity, and wind speed. Among these parameters, dew point, pressure, temperature, and visibility exhibited the highest influence, each contributing more than 10% to the feature importance. Following them, relative humidity and wind speed contributed more than 5% each. The hour of the day ranked as the second-to-last feature in terms of importance, reflecting the diurnal evolution of the vertical structure of NO_2. Precipitation had the least impact on the model, with an importance value of 3.27%. Our prediction through the RF model has shown a good agreement between the predicted and measured data for the 10-fold cross-validation and the fully-trained model. These results reveal the great impacts of meteorological values on the vertical structure of NO_2.

Ground-level NO_2 concentrations are more critical in air quality and health risk studies compared to satellite columnar measurements. The mixing height of NO_2 is an essential factor for converting the satellite-derived VCDs of NO_2 to ground-level NO_2 concentration. Several studies have utilized different methods, such as air quality models, machine learning techniques, land use regression, and geographically weighted regression, to convert satellite columnar measurements to ground-level NO_2 concentrations. In previous studies, the PBL height has been used as a significant factor in linking the two variables due to its ability to regulate the vertical distribution of air pollutants (Lamsal et al., 2008; Wei et al., 2022; Zhu et al., 2019). With an improved understanding of the mixing height of NO_2, future study can improve the conversions from satellite columnar measurements to ground-level NO_2 concentrations.

The GEMS measurements exhibit certain uncertainties and limitations. One of the primary factors affecting the reliability of GEMS measurements is the presence of cloudy conditions. Due to the high level of uncertainty associated with satellite observations under such conditions, data with a cloud fraction exceeding 30% were excluded from the analysis. This exclusion aimed to strike a balance between obtaining sufficient measurements and minimizing the influence of cloud-contaminated data. Data with a solar zenith angle exceeding 70° were also excluded from consideration. Fig. S2 illustrates that the size of the valid sample decreases in regions with a higher likelihood of cloud cover. Furthermore, the sample size is relatively small in the early morning due to the absence of solar radiation. This limitation is inherent to satellite measurements since there are no measurements available during the night. The nominal detection limit for the VCDs of NO_2 products is set at 1×10^{14} molec/cm^2. Any VCDs of NO_2 greater than 1×10^{17} molec/cm^2 were deemed noise and thus removed from the analysis. Moreover, the evaluation of the GEMS data using ground MAX-DOAS measurements revealed a possible overestimate under clean conditions and an underestimate under polluted conditions. The data employed in this study corresponds to version 1 of the GEMS product. Continuous efforts are underway to enhance the accuracy of GEMS products. It is expected that future versions will offer improved quality and reliability.

5. Conclusion

In this study, we introduced the concept of the mixing height of NO_2 to indicate the vertical structure of NO_2 within the atmosphere. A comprehensive investigation of the mixing height of NO_2 was performed based on the measurements from GEMS and ground monitoring networks. The impacts of the meteorological parameters on the mixing height of NO_2 were investigated. Then, the machine learning-based random forest model was used to predict the mixing height of NO_2 from various meteorological values. The mixing height of NO_2 demonstrated a significant seasonal variation pattern, with the highest levels in summer and the lowest levels in winter. In addition, it increased from early morning to midafternoon. The investigation of the meteorological effects showed that the mixing height of NO_2 was positively associated with temperature and wind speed. However, it was negatively associated with relative humidity and air pressure. The modelled mixing height from the machine learning showed a good agreement with those obtained from measurements. These analyses indicate the significant impacts of meteorological conditions on the vertical structure of NO_2. The results underscore the great capability of the new-generation geostationary satellite of enhancing our understanding of the three-dimensional variation in NO_2 over a large region.

Credit author statement

Supervision: AKH Lau. Analysis and draft: Naveed Ahmad. Conceptualization: CQ Lin. Data curation: Jhoon Kim, Kai Qin. Funding acquisition: Chengcai Li. Review and editing: Chunsheng Zhao, Jintai Lin, Jimmy CH Fung, Ying Li.

Declaration of competing interest

The authors declare that they have no known competing financial interests or personal relationships that could have appeared to influence the work reported in this paper.

Data availability

Data will be made available on request.

Acknowledgements

This work was supported by the NSFC/RGC Joint Research Project (Grant Nos. 42161160329 and N_HKUST609/21) and the Research Grants Council of Hong Kong (Project Nos. GRF 16202120 and T24/504/17). We thank the National Institute of Environmental Research (NIER) of South Korea for providing the GEMS data (https://nesc.nier.go.kr). We thank the Institute for the Environment (IENV) and Environmental Central Facility (ENVF) of the Hong Kong University of Science and Technology (HKUST) for providing atmospheric and environmental data (http://envf.ust.hk/dataview/). The authors declare that they have no actual or potential competing financial interests.

Appendix A. Supplementary data

Supplementary data to this article can be found online at https://doi.org/10.1016/j.chemosphere.2023.140615.

References

Akther, T., Rappenglueck, B., Osibanjo, O., Retama, A., Rivera-Hernández, O., 2023. Ozone precursors and boundary layer meteorology before and during a severe ozone episode in Mexico city. Chemosphere 318, 137978. https://doi.org/10.1016/j.chemosphere.2023.137978.

Amann, M., Kiesewetter, G., Schöpp, W., Klimont, Z., Winiwarter, W., Cofala, J., Rafaj, P., Höglund-Isaksson, L., Gomez-Sabriana, A., Heyes, C., Purohit, P., Borken-Kleefeld, J., Wagner, F., Sander, R., Fagerli, H., Nyiri, A., Cozzi, L., Pavarini, C., 2020. Reducing global air pollution: the scope for further policy interventions: achieving clean air worldwide. Phil. Trans. Math. Phys. Eng. Sci. 378 (2183), 1–27. https://doi.org/10.1098/rsta.2019.0331.

Bourgeois, I., Peischl, J., Neuman, J.A., Brown, S.S., Allen, H.M., Campuzano-Jost, P., Coggon, M.M., DiGangi, J.P., Diskin, G.S., Gilman, J.B., Gkatzelis, G.I., Guo, H., Halliday, H.A., Hanisco, T.F., Holmes, C.D., Huey, L.G., Jimenez, J.L., Lamplugh, A. D., Lee, Y.R., et al., 2022. Comparison of airborne measurements of NO, NO2, HONO, NOy, and CO during FIREX-AQ. Atmos. Meas. Tech. 15 (16), 4901–4930. https://doi.org/10.5194/amt-15-4901-2022.

Cheng, S., Jin, J., Ma, J., Lv, J., Liu, S., Xu, X., 2022. Temporal variation of NO2 and HCHO vertical profiles derived from MAX-DOAS observation in summer at a rural site of the north China plain and ozone production in relation to HCHO/NO2 ratio. Atmosphere 13 (6), 860. https://doi.org/10.3390/atmos13060860.

Chong, J., Kim, Y.J., Gu, M., Wagner, T., Song, C.H., 2016. Mobile MAX-DOAS observation of NO2 and comparison with OMI satellite data in the western coastal areas of the Korean peninsula. Chemosphere 143, 10–16. https://doi.org/10.1016/j.chemosphere.2015.06.071.

Chow, E.C., Li, R.C., Zhou, W., 2018. Influence of tropical cyclones on Hong Kong air quality. Adv. Atmos. Sci. 35, 1177–1188. https://doi.org/10.1007/s00376-018-7225-4.

Flynn, L., Long, C., Wu, X., Evans, R., Beck, C.T., Petropavlovskikh, I., McConville, G., Yu, W., Zhang, Z., Niu, J., Beach, E., Hao, Y., Pan, C., Sen, B., Novicki, M., Zhou, S., Seftor, C., 2014. Performance of the ozone mapping and profiler suite (OMPS) products. J. Geophys. Res. Atmos. 119 (10), 6181–6195. https://doi.org/10.1002/2013JD020467.

Guo, F., Ju, X., Bao, M., Lu, G., Liu, Z., Li, Y., Mu, Y., 2017. Relationship between lightning activity and tropospheric nitrogen dioxide and the estimation of lightning-produced nitrogen oxides over China. Adv. Atmos. Sci. 34 (2), 235–245. https://doi.org/10.1007/s00376-016-6087-x.

Guo, J., Miao, Y., Zhang, Y., Liu, H., Li, Z., Zhang, W., He, J., Lou, M., Yan, Y., Bian, L., Zhai, P., 2016. The climatology of planetary boundary layer height in China derived from radiosonde and reanalysis data. Atmos. Chem. Phys. 16 (20), 13309–13319. https://doi.org/10.5194/acp-16-13309-2016.

Hastie, T., Tibshirani, R., Friedman, J., 2008. Springer Series in Statistics the Elements of Statistical Learning Data Mining, Inference, and Prediction, 10.1007/b94608.

Holzworth, G.C., 1964. Estimates of mean maximum mixing depths in the contiguous United States. Mon. Weather Rev. 92 (5), 235–242. https://doi.org/10.1175/1520-0493(1964)092<0235:EOMMMD>2.3.CO;2.

Hong, Q., Liu, C., Hu, Q., Xing, C., Tan, W., Liu, H., Huang, Y., Zhu, Y., Zhang, J., Geng, T., Liu, J., 2019. Evolution of the vertical structure of air pollutants during winter heavy pollution episodes: the role of regional transport and potential sources. Atmos. Res. 228, 206–222. https://doi.org/10.1016/j.atmosres.2019.05.016.

Huang, Y., Guo, B., Sun, H., Liu, H., Chen, S.X., 2021. Relative importance of meteorological variables on air quality and role of boundary layer height. Atmos. Environ. 267, 118737. https://doi.org/10.1016/j.atmosenv.2021.118737.

Iqbal, A., Ahmad, N., Din, H.M.U., Roozendael, M. Van, Anjum, M.S., Khan, M.Z.A., Khokhar, M.F., 2022. Retrieval of NO2 columns by exploiting MAX-DOAS observations and comparison with OMI and TROPOMI data during the time period of 2015– 2019. Aerosol Air Qual. Res. 22 (6), 210398 https://doi.org/10.4209/aaqr.210398.

Jacob, D., 2000. Heterogeneous chemistry and tropospheric ozone. Atmos. Environ. 34 (12–14), 2131–2159. https://doi.org/10.1016/S1352-2310(99)00462-8.

Jion, Most. M. M. F., Jannat, J.N., Mia, Md Y., Ali, Md A., Islam, Md S., Ibrahim, S.M., Pal, S.C., Islam, A., Sarker, A., Malafaia, G., Bilal, M., Islam, A.R.M.T., 2023. A critical review and prospect of NO2 and SO2 pollution over Asia: hotspots, trends, and sources. Sci. Total Environ. 876, 162851 https://doi.org/10.1016/j.scitotenv.2023.162851.

Kalmus, P., Ao, C.O., Wang, K.N., Manzi, M.P., Teixeira, J., 2022. A high-resolution planetary boundary layer height seasonal climatology from GNSS radio occultations. Rem. Sens. Environ. 276, 113037 https://doi.org/10.1016/j.rse.2022.113037.

Kang, Y., Tang, G., Li, Q., Liu, B., Cao, J., Hu, Q., Wang, Y., 2021. Evaluation and evolution of MAX-DOAS-observed vertical NO2 profiles in urban Beijing. Adv. Atmos. Sci. 38 (7), 1188–1196. https://doi.org/10.1007/s00376-021-0370-1.

Karagkiozidis, D., Koukouli, M.E., Bais, A., Balis, D., Tzoumaka, P., 2023. Assessment of the NO2 spatio-temporal variability over Thessaloniki, Greece, using MAX-DOAS measurements and comparison with S5P/TROPOMI observations. Appl. Sci. 13 (4), 2641. https://doi.org/10.3390/app13042641.

Kim, J., Jeong, U., Ahn, M.H., Kim, J.H., Park, R.J., Lee, H., Song, C.H., Choi, Y.S., Lee, K. H., Yoo, J.M., Jeong, M.J., Park, S.K., Lee, K.M., Song, C.K., Kim, S.W., Kim, Y.J., Kim, S.W., Kim, M., Go, S., et al., 2020. New era of air quality monitoring from space: geostationary environment monitoring spectrometer (GEMS). Bull. Am. Meteorol. Soc. 101 (1), E1–E22. https://doi.org/10.1175/BAMS-D-18-0013.1.

Koelemeijer, R.B.A., Homan, C.D., Matthijsen, J., 2006. Comparison of spatial and temporal variations of aerosol optical thickness and particulate matter over Europe. Atmos. Environ. 40 (27), 5304–5315. https://doi.org/10.1016/j.atmosenv.2006.04.044.

Kreher, K., Van Roozendael, M., Hendrick, F., Apituley, A., Dimitropoulou, E., Frieß, U., Richter, A., Wagner, T., Lampel, J., Abuhassan, N., Ang, L., Anguas, M., Bais, A., Benavent, N., Bösch, T., Bognar, K., Borovski, A., Bruchkouski, I., Cede, A., et al., 2020. Intercomparison of NO2, O4, O3 and HCHO slant column measurements by MAX-DOAS and zenith-sky UV-visible spectrometers during CINDI-2. Atmos. Meas. Tech. 13 (5), 2169–2208. https://doi.org/10.5194/amt-13-2169-2020.

Lamsal, L.N., Martin, R.V., van Donkelaar, A., Steinbacher, M., Celarier, E.A., Bucsela, E., Dunlea, E.J., Pinto, J.P., 2008. Ground-level nitrogen dioxide concentrations inferred from the satellite-borne Ozone Monitoring Instrument. J. Geophys. Res. Atmos. 113 (16), 1–15. https://doi.org/10.1029/2007JD009235.

Levi, Y., Dayan, U., Levy, I., Broday, D.M., 2020. On the association between characteristics of the atmospheric boundary layer and air pollution concentrations. Atmos. Res. 231, 104675 https://doi.org/10.1016/j.atmosres.2019.104675.

Li, C., Managi, S., 2022. Estimating monthly global ground-level NO2 concentrations using geographically weighted panel regression. Rem. Sens. Environ. 280, 113152 https://doi.org/10.1016/j.rse.2022.113152.

Li, L., Lu, C., Chan, P.W., Zhang, X., Yang, H.L., Lan, Z.J., et al., 2020. Tower observed vertical distribution of PM2. 5, O3 and NOx in the Pearl River Delta. Atmos. Environ. 220, 117083 https://doi.org/10.1016/j.atmosenv.2019.117083.

Li, M., Mao, J., Chen, S., Bian, J., Bai, Z., Wang, X., et al., 2022. Significant contribution of lightning NOx to summertime surface O3 on the Tibetan Plateau. Sci. Total Environ. 829, 154639 https://doi.org/10.1016/j.scitotenv.2022.154639.

Lin, C., Leung, K.K., Alfred, L.C., Tsang, R.C., Tsui, W.B., Fung, J.C., et al., 2021. Effects of synoptic patterns on the vertical structure of ozone in Hong Kong using lidar measurement. Atmos. Environ. 257, 118490 https://doi.org/10.1016/j.atmosenv.2021.118490.

Liu, Y., Sarnat, J.A., Kilaru, V., Jacob, D.J., Koutrakis, P., 2005. Estimating ground-level PM2.5 in the eastern United States using satellite remote sensing. Environ. Sci. Technol. 39 (9), 3269–3278. https://doi.org/10.1021/es049352m.

Myhre, G., Shindell, D., Bréon, F.-M., Collins, W., Fuglestvedt, J., Huang, J., Koch, D., Lamarque, J.-F., Lee, D., Mendoza, B., Nakajima, T., Robock, A., Stephens, G., Takemura, T., Zhang, H., 2013. Anthropogenic and natural radiative forcing. In: Stocker, T.F., et al. (Eds.), Climate Change 2013: the Physical Science Basis. Contribution of Working Group I to the Fifth Assessment Report of the Intergovernmental Panel on Climate Change. Editied. Cambridge University Press, Cambridge, United Kingdom and New York, NY, USA.

Park, H., Jeong, S., Park, H., Labzovskii, L.D., Bowman, K.W., 2021. An assessment of emission characteristics of Northern Hemisphere cities using spaceborne observations of CO2, CO, and NO2. Rem. Sens. Environ. 254, 112246 https://doi.org/10.1016/j.rse.2020.112246.

Platt, U., Stutz, J., Platt, U., Stutz, J., 2008. Differential Absorption Spectroscopy. Springer Berlin Heidelberg, pp. 135–174. https://doi.org/10.1007/978-3-540-75776-4 6.

Seidel, D.J., Zhang, Y., Beljaars, A., Golaz, J.C., Jacobson, A.R., Medeiros, B., 2012. Climatology of the planetary boundary layer over the continental United States and Europe. J. Geophys. Res. Atmos. 117 (17) https://doi.org/10.1029/2012JD018143.

Shah, V., Jacob, D.J., Moch, J.M., Wang, X., Zhai, S., 2020. Global modeling of cloud water acidity, precipitation acidity, and acid inputs to ecosystems. Atmos. Chem. Phys. 20 (20), 12223–12245. https://doi.org/10.5194/acp-20-12223-2020.

Su, T., Li, J., Li, C., Xiang, P., Lau, A.K.H., Guo, J., et al., 2017. An intercomparison of long-term planetary boundary layer heights retrieved from CALIPSO, ground-based lidar, and radiosonde measurements over Hong Kong. J. Geophys. Res. Atmos. 122 (7), 3929–3943. https://doi.org/10.1002/2016JD025937.

Su, T., Li, Z., Kahn, R., 2020. A new method to retrieve the diurnal variability of planetary boundary layer height from lidar under different thermodynamic stability conditions. Rem. Sens. Environ. 237, 111519 https://doi.org/10.1016/j.rse.2019.111519.

Van Der A, R.J., Eskes, H.J., Boersma, K.F., Van Noije, T.P.C., Van Roozendael, M., De Smedt, I., et al., 2008. Trends, seasonal variability and dominant NOx source derived from a ten year record of NO2 measured from space. J. Geophys. Res. Atmos. 113 (D4) https://doi.org/10.1029/2007JD009021.

Veefkind, J.P., Aben, I., McMullan, K., Förster, H., de Vries, J., Otter, G., Claas, J., Eskes, H.J., de Haan, J.F., Kleipool, Q., van Weele, M., Hasekamp, O., Hoogeveen, R., Landgraf, J., Snel, R., Tol, P., Ingmann, P., Voors, R., Kruizinga, B., et al., 2012. TROPOMI on the ESA Sentinel-5 Precursor: a GMES mission for global observations of the atmospheric composition for climate, air quality and ozone layer applications. Rem. Sens. Environ. 120, 70–83. https://doi.org/10.1016/j.rse.2011.09.027.

Wang, R., Bei, N., Pan, Y., Wu, J., Liu, S., Li, X., et al., 2023. Urgency of controlling agricultural nitrogen sources to alleviate summertime air pollution in the North China Plain. Chemosphere 311, 137124. https://doi.org/10.1016/j.chemosphere.2022.137124.

Wang, S., Li, C., Zhou, H., 2019. Impact of China's economic growth and energy consumption structure on atmospheric pollutants: based on a panel threshold model. J. Clean. Prod. 236, 117694 https://doi.org/10.1016/j.jclepro.2019.117694.

Wang, T., Xue, L., Feng, Z., Dai, J., Zhang, Y., Tan, Y., 2022. Ground-level ozone pollution in China: a synthesis of recent findings on influencing factors and impacts. Environ. Res. Lett. 17 (6), 063003 https://doi.org/10.1088/1748-9326/ac69fe.

Wei, J., Liu, S., Li, Z., Liu, C., Qin, K., Liu, X., Pinker, R.T., Dickerson, R.R., Lin, J., Boersma, K.F., Sun, L., Li, R., Xue, W., Cui, Y., Zhang, C., Wang, J., 2022. Ground-level NO2Surveillance from space across China for high resolution using interpretable spatiotemporally weighted artificial intelligence. Environ. Sci. Technol. 56 (14), 9988–9998. https://doi.org/10.1021/acs.est.2c03834.

Xiang, Y., Zhang, T., Liu, J., Lv, L., Dong, Y., Chen, Z., 2019. Atmosphere boundary layer height and its effect on air pollutants in Beijing during winter heavy pollution. Atmos. Res. 215, 305–316. https://doi.org/10.1016/j.atmosres.2018.09.014.

Yang, L.H., Jacob, D.J., Colombi, N.K., Zhai, S., Bates, K.H., Shah, V., Beaudry, E., Yantosca, R.M., Lin, H., Brewer, J.F., Chong, H., Travis, K.R., Crawford, J.H., Lamsal, L.N., Koo, J.-H., Kim, J., 2023. Tropospheric NO_2 vertical profiles over South Korea and their relation to oxidant chemistry: implications for geostationary satellite retrievals and the observation of NO_2 diurnal variation from space. Atmos. Chem. Phys. 23 (4), 2465–2481. https://doi.org/10.5194/acp-23-2465-2023.

Yin, J., Gao, C.Y., Hong, J., Gao, Z., Li, Y., Li, X., Fan, S., Zhu, B., 2019. Surface meteorological conditions and boundary layer height variations during an air pollution episode in Nanjing, China. J. Geophys. Res. Atmos. 124 (6), 3350–3364. https://doi.org/10.1029/2018JD029848.

Zhang, X., Zhang, W., Lu, X., Liu, X., Chen, D., Liu, L., Huang, X., 2018. Long-term trends in NO2 columns related to economic developments and air quality policies from 1997 to 2016 in China. Sci. Total Environ. 639, 146–155. https://doi.org/10.1016/j.scitotenv.2018.04.435.

Zhang, Y.L., Cao, F., 2015. Fine particulate matter (PM2. 5) in China at a city level. Sci. Rep. 5 (1), 1–12. https://doi.org/10.1038/srep14884.

Zhao, S., Liu, S., Sun, Y., Liu, Y., Beazley, R., Hou, X., 2020. Assessing NO2-related health effects by non-linear and linear methods on a national level. Sci. Total Environ. 744, 140909 https://doi.org/10.1016/j.scitotenv.2020.140909.

Zhu, Y., Zhan, Y., Wang, B., Li, Z., Qin, Y., Zhang, K., 2019. Spatiotemporally mapping of the relationship between NO2 pollution and urbanization for a megacity in Southwest China during 2005–2016. Chemosphere 220, 155–162. https://doi.org/10.1016/j.chemosphere.2018.12.095.